13. LaRoche, J., Murray, H., Orellana, M. & Newton, J. *J. Phycol.* **31,** 520–530 (1995).
14. Doucette, G. J., Erdner, D. L., Peleato, M. L., Hartman, J. J. & Anderson, D. M. *Mar. Ecol. Prog. Ser.* **130,** 269–276 (1996).
15. Coale, K. H., Fitzwater, S. E., Gordon, R. M., Johnson, K. S. & Barber, R. T. *Nature* **379,** 621–624 (1996).
16. Kolber, Z. S. *et al. Nature* **371,** 145–149 (1994).
17. Behrenfeld, M. J., Bale, T., Aiken, J., Kolber, Z. S. & Falkowski, P. G. *Eos* **76,** OS176 (1996).
18. Booth, B. C., Lewin, J. & Postel, J. R. *Prog. Oceanogr.* **32,** 57–99 (1993).
19. Sunda, W. G. & Huntsman, S. A. *Mar. Chem.* **50,** 189–206 (1995).
20. Wells, M. L., Price, N. M. & Bruland, K. W. *Mar. Chem.* **48,** 157–182 (1995).
21. Barbeau, K., Moffett, J. W., Caron, D. A., Croot, P. L. & Erdner, D. L. *Nature* **380,** 61–64 (1996).
22. Wu, J. & Luther, G. W. *Mar. Chem.* **50,** 159–177 (1995).
23. Entsch, B., Sim, R. G. & Hatcher, D. G. *Mar. Biol.* **73,** 17–30 (1983).
24. Yang, L. thesis, Univ. British Columbia (1993).
25. Martin, J. H., Gordon, R. M., Fitzwater, S. & Broenkow, W. W. *Deep Sea Res.* **35,** 177–196 (1989).
26. Rabilloud, T., Carpentier, G. & Tarroux, P. *Electrophoresis* **9,** 288–291 (1988).
27. Towbin, H., Staehelin, T. & Gordon, J. *Proc. Natl Acad. Sci. USA* **76,** 4350–4354 (1979).
28. Lin, S., Chang, J. & Carpenter, E. J. *J. Phycol.* **31,** 388–395 (1995).

ACKNOWLEDGEMENTS. We thank J. Berges, A. Milligan, H. Murray-Fobin, F. Whitney, R. Walker and the officers and crew of the RV *John P. Tully* for their assistance, R. Chretien for determinations of DFe made on samples collected by P.W.B. and P. J. Falkowski for the Rubisco antiserum. D. Wallace, P. J. Harrison and T. Pedersen provided helpful comments and discussions. This research was supported by the NSF (R.J.G. and G. W. Luther), the US Department of Energy Office of Health and Environmental Research (J.L.), and by the NSERC (Canada) JGOFS programme (P.W.B. and P. J. Harrison).

CORRESPONDENCE and requests for materials should be addressed to J.L.R. (e-mail: Laroche @BNLUX1.BNL.GOV).

Two different areas within the primary motor cortex of man

Stefan Geyer*, Anders Ledberg†, Axel Schleicher‡, Shigeo Kinomura†, Thorsten Schormann‡, Uli Bürgel‡, Torkel Klingberg†, Jonas Larsson†, Karl Zilles*‡ & Per E. Roland†

* Department of Neuroanatomy and ‡ C. and O. Vogt Institute for Brain Research, Heinrich Heine University Düsseldorf, P. O. Box 101007, 40001 Düsseldorf, Germany
† Division of Human Brain Research, Department of Neuroscience, The Karolinska Institute, Doktorsringen 6F, 17177 Stockholm, Sweden

The primary motor area (M1) of mammals has long been considered to be structurally and functionally homogeneous[1–5]. This area corresponds to Brodmann's cytoarchitectural area 4. A few reports showing that arm and hand are doubly represented in M1 of macaque monkeys[6,7] and perhaps man[8], and that each subarea has separate connections from somatosensory areas, have, with a few exceptions[9–12], gone largely unnoticed. Here we show that area 4 in man can be subdivided into areas '4 anterior' (4a) and '4 posterior' (4p) on the basis of both quantitative cytoarchitecture and quantitative distributions of transmitter-binding sites. We also show by positron emission tomography that two representations of the fingers exist, one in area 4a and one in area 4p. Roughness discrimination activated area 4p significantly more than a control condition of self-generated movements. We therefore suggest that the primary motor area is subdivided on the basis of anatomy, neurochemistry and function.

We analysed sections of five human brains with quantitative cytoarchitectonic methods[13]. The border between somatosensory area 3a and the posterior part of area 4 was sharp. Large, slender pyramidal neurons in layer III characterized area 6, and the transition to the anterior part of area 4 was distinct. Differences in volume densities of neurons in layers II to VI between areas 3a and 4 as well as between 6 and 4 were statistically significant (Fig. 1). Our quantitative methods also revealed a statistically significant difference between the laminar density of neurons in the posterior part of area 4, area 4p and its anterior part, area 4a (Fig. 1). Area 4a contained slightly larger, more densely packed pyramidal cells in layer III than did 4p. Differences between 4a and 4p were also detected by *in vitro* receptor autoradiography. Both regional and laminar densities of [^{3}H]oxotremorine-M binding sites (muscarinic M_2 and M_4 receptors) were much higher in 4p than in 4a (Fig. 2*a*). There was a clear border between these areas which corresponded exactly to one marking differences in laminar densities of neurons in an adjacent Nissl section (Fig. 2*b*). Another

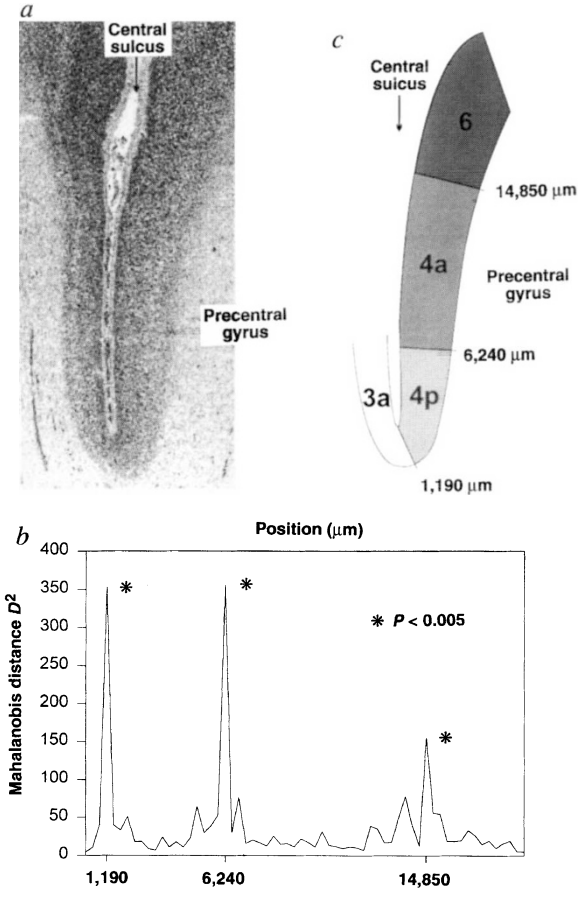

FIG. 1 Quantitative cytoarchitecture of area 4. *a*, Grey-level index image showing densities of neurons in a Nissl-stained section through pre- and postcentral gyrus, roughly half-way between interhemispheric and Sylvian fissures. *b*, Plot of Mahalanobis distance D^2 as a function of length measured along the middle of layer IV. At positions 1,190, 6,240 and 14,850 μm from the bottom of the sulcus, the cytoarchitecture changes significantly. These positions correspond to borders between areas 3a/4p, 4p/4a and 4a/6, as shown in *c*.
METHODS. Coronal 20-μm paraffin sections were stained with a modified Nissl method[21]. Volume density of cells was estimated with the grey-level index (GLI) procedure[13]. Each pixel represents neuronal density in a field measuring 27 μm per side. Density profiles, oriented orthogonally to the laminae and extending from the boundary between layers I and II to that between layer VI and white matter were extracted from the images. Profiles were standardized to a cortical depth of 100%. Each profile was 11 pixels (297 μm) wide, that is each value in a profile represents the average of 11 GLI values. Spacing between profiles was 297 μm. Characterizing features were extracted from each profile. They included the mean amplitude and the first 4 moments (mean, s.d., skewness, kurtosis). A mean feature vector $\overline{\boldsymbol{X}_1}$ was calculated from a block of 10 adjacent profiles, and another mean feature vector $\overline{\boldsymbol{X}_2}$ from a neighbouring block of 10 profiles. The Mahalanobis distance[22] $D^2 = (\overline{\boldsymbol{X}_1} - \overline{\boldsymbol{X}_2})'\boldsymbol{C}^{-1}(\overline{\boldsymbol{X}_1} - \overline{\boldsymbol{X}_2})$ was calculated from the vectors and the inverse of the pooled covariance matrix $\boldsymbol{C}^{-1}$. Plotting the D^2 values as a function of the position of the blocks of profiles revealed maxima at locations at which regions covered by profiles showed large differences in laminar patterns. Statistical significance was established by computing Hotelling's statistic $T^2 = D^2/(1/n_1 + 1/n_2)$ in which $n_1 = n_2 = 10$, the number of profiles from which each of the mean vectors had been calculated. The corresponding P value was not corrected for multiple comparisons, as the probability of getting three such maxima at the predicted locations in a set of adjoining sections is exceedingly small.

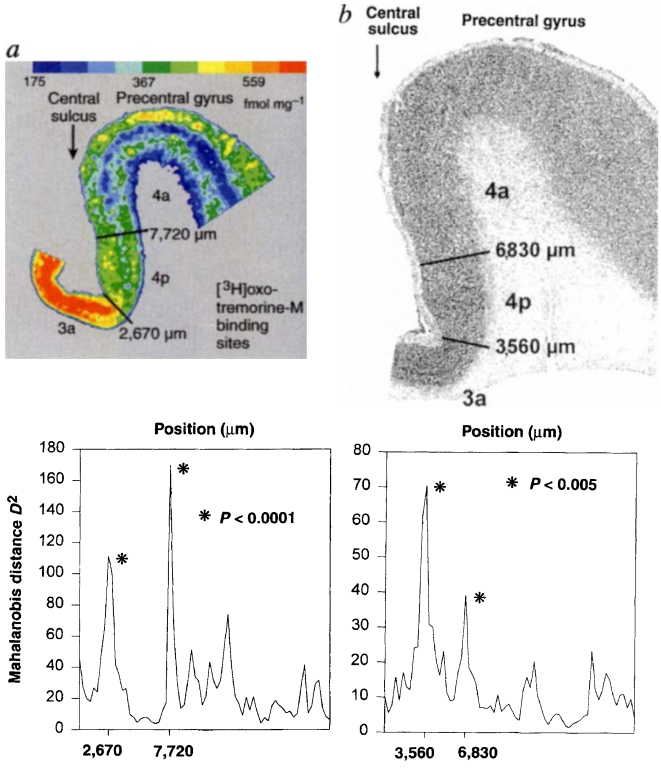

FIG. 2 *a*, Contrast-enhanced, colour-coded autoradiograph of section through precentral gyrus showing distribution of [^{3}H]oxotremorine-M binding sites on muscarinic M_2 and M_4 receptors (upper panel). B_{max} values expressed as fmol per mg protein. *b*, GLI image (see Fig. 1) of Nissl-stained adjacent section (upper panel). Observer-independent mapping revealed statistically significant maxima in Mahalanobis distance D^2 (ordinate; $P < 0.0001$ and $P < 0.005$) at positions 2,670 and 7,720 µm (abscissa) from bottom of sulcus in autoradiograph (*a*, lower panel) and at positions 3,560 and 6,830 µm in GLI plot (*b*, lower panel). These positions represent borders between areas 3a/4p and 4p/4a, respectively. Border between 4a and 6 not shown.

METHODS. Fresh, unfixed tissue was sectioned with a cryostat (20 µm). For GLI procedure, see Fig. 1. [^{3}H]oxotremorine-M binding sites (total binding) were labelled by quantitative *in vitro* receptor autoradiography[23]. Autoradiographs were digitized with a CCD-camera. Standards of known radioactivity were used to compute a transformation curve indicating the relationship between grey values in the autoradiograph and concentrations of radioactivity in the tissue. Concentration values were multiplied by $(K_d + c)/c$ (K_d, equilibrium dissociation constant of ligand-binding kinetics = 1.74 nM; *c*, free concentration of labelled ligand = 0.86 nM) to obtain B_{max} values. Non-specific binding, determined by [^{3}H]oxotremorine-M labelling in the presence of 1 µM of unlabelled carbachol, was less than 5% of total binding. After calculating B_{max} values, autoradiographs were subjected to linear contrast enhancement, colour coding and median filtering (matrix size 5 × 5 pixels). Equidistant density profiles (297 µm wide), extending from the pial surface to the layer VI/white matter boundary, were extracted from the original data. They were oriented perpendicularly to lines drawn at these limits and standardized to a cortical depth of 100%. D^2 and significance of maxima were calculated as described for Fig. 1.

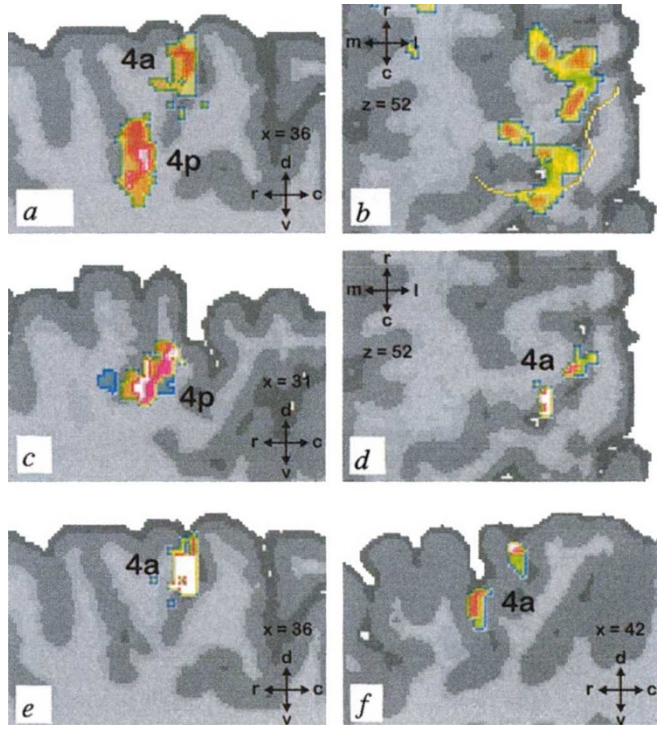

FIG. 3 Images of the standard brain with cytoarchitecture and functional activations in identical anatomical format[14]. *a*, Sagittal section 36 mm to the left of the midline ($x = 36$) showing those regions in which 4a and 4p were located in at least 3 of 5 brains. Yellow: overlap in 3 of 5 brains, red: 4 of 5, white: 5. r, rostral; c, caudal; d, dorsal; v, ventral. *b*, Horizontal section 52 mm above the midcommissural plane ($z = 52$), showing two activations in the left hemisphere associated with rapid flexions of the right thumb in the cortex lining the anterior wall of the central sulcus (somatosensory reaction-time task). The average course of the central sulcus is also shown. m, medial; l, lateral. *c*, Sagittal section ($x = 31$) showing in area 4p the overlapping activations of the two reaction-time tasks (thumb), roughness discrimination (thumb and index finger), and discrimination of ellipsoids (mainly thumb, index and middle finger). White: all tasks overlap; red: overlap of roughness discrimination and ellipsoid discrimination; yellow: overlap of ellipsoid discrimination and one of the reaction-time tasks. Centres of gravity (*x*, *y*, *z*): overlap of the two reaction-time tasks, 33, −27, 50; overlap of all tasks, 33, −28, 50. *d*, Horizontal section ($z = 52$) showing the overlap within area 4a (white; 38, −22, 55) of visual-memory task (index and middle finger) and ellipsoid discrimination (thumb, index and middle finger). *e*, Sagittal section ($x = 36$) showing the overlap in area 4a (white) of visual-memory task and ellipsoid discrimination. *f*, Sagittal section ($x = 42$) showing the overlap of activations of the two reaction-time tasks (thumb; lower region, 42, −13, 52) and another overlap between the two reaction time tasks (thumb) and ellipsoid discrimination (thumb, index and middle finger; upper region), both within area 4a. The localization of the overlaps within 4a and 4p were determined by Boolean operations on the images, thus *c*–*f* show only those parts of the overlaps which belonged to the space defined in *a*.

METHODS. Tasks: First group ($n = 10$): two reaction-time tasks (control state, complete rest[24]); visual, key press with right thumb in response to a change in luminance of a yellow monochrome circle; somatosensory, key press at the protrusion of a stylus to the tip of the right index finger. Second group ($n = 10$): visual memory task; key press with right index or middle finger depending on which of two pictures belonged to a previously learned picture pair (visually matched control, no movement). Third group ($n = 9$): tactile discrimination of shapes of two ellipsoids with fingers of the right hand by a two-alternative forced-choice procedure[18] (control, rest with eyes fixating a cross on the screen hiding the ellipsoids). Fourth group ($n = 9$): discrimination of roughness of two polyoxymethylene cylinders with different microprofiles with right thumb and index finger by a two-alternative forced-choice procedure[18]. All subjects and brains were scanned with a 1.5 T magnetic resonance (MR) scanner with 3D-spoiled gradient (3D-SPGR) or 3D-fast low angle shot (3D-FLASH) pulse sequences giving 1 mm^3 isotropic voxels. For PET methods and treatment of data see refs. 17, 25. Scans of regional cerebral blood flow (rCBF) were obtained with an in-plane spatial resolution of 4.5 mm and an interslice distance of 6.5 mm. Subjects received a bolus injection of 70 mCi of [^{15}O]butanol. Arterial tracer radioactivity was continuously monitored and rCBF values calculated on the basis of data collected during the first 60 s after injection[25]. rCBF images were anatomically standardized as described above[17]. Final image resolution was 4.2 mm in plane[25]. Subtraction images were made by voxel-by-voxel subtraction of control rCBF conditions from motor conditions. Only clusters of high *t*-value having a probability of less than 0.05 of being false positives within the space of the brain were considered statistically significant[25]. The probability that such clusters should be localized to the space covered by areas 4a and 4p is then less than 0.0005.

corresponding border within Brodmann's area 4 separated areas with differing densities of [^{3}H]ketanserin-binding sites[14] (mainly serotoninergic 5-HT$_2$ receptors; data not shown). The images of the sections of both cytoarchitectonic and autoradiographic studies were transformed into standard anatomical format by the computerized Human Brain Atlas[14–17] so that structural findings could be compared with those of the positron emission tomography (PET) studies. An overlay map was calculated and area 4a and 4p were defined as the space of the brain within which area 4a or 4p could be found in at least three of five brains (Fig. 3*a*).

To test whether the two subareas differed functionally we analysed PET activations of M1 in four groups of normal right-handed subjects performing different motor actions with the fingers of the right hand (Fig. 3). The hypotheses were (1) that double representations of the fingers might exist (as suggested in refs 6, 7) and (2) that externally triggered movements and movements guided by somatosensory information might activate area 4a and 4p differentially. The PET images were transformed into the standard format of the computerized brain atlas, as were the images of the structural studies. We then checked whether the locations of the PET activations were within areas 4a or 4p (Fig. 3).

In reaction-time tasks, subjects pressed a response key with their right thumb. The somatosensory reaction-time task (response to touch on right index finger) activated two separate fields within M1, one located medially within area 4p, and one more superiorly and laterally within 4a (Fig. 3*b*). In this task, the movement, a thumb flexion to press the key, was not guided by the tactile stimulus, in the sense that it did not provide any information about how the thumb flexion should be performed. In a visual reaction-time task, activation of areas 4a and 4p overlapped the active regions of the somatosensory reaction-time task (Fig 3*c*,*f*). This indicates that two different representations of the thumb might exist. In a tactile discrimination task the subjects examined ellipsoids with complex, learned, stereotypical movements in which mainly the thumb, index and middle finger were active[18–20]. The trajectories of the fingers were guided by the curvatures of the objects[18,19]. Although most of the activation was localized to area 4p, overlapping the activations of the reaction-time tasks (Fig. 3*c*), a separate overlap was also found between the 4a reaction-time task activation and the tactile discrimination task (Fig. 3*f*). The probability that such activations from two independent studies by chance should overlap both in area 4a and in area 4p was very small. This seems to confirm that two different representations of the thumb exist.

In a visual memory task (Fig. 3, legend), the subjects used the index and middle finger for responses. This activated area 4a in regions overlapping the tactile discrimination activation but not those associated with the reaction-time tasks (Fig. 3*d*, *e*). Finally, in a roughness discrimination task, the subjects using the thumb and index finger showed activation in area 4p in almost exactly the same territory as in the tactile discrimination task (Fig. 3*c*). This indicates that also two representations of the index finger and presumably also the middle finger exist: one within area 4a and one within area 4p. A clue to a possible separation of function arose from the observation that roughness discrimination did not activate area 4a, but activated area 4p significantly more than the control condition of self-generated movements ($P < 0.05$).

We have described two structurally different areas in the primary motor cortex, 4a and 4p, each having one representation of the thumb, index and possibly middle finger. These areas differ cytoarchitecturally, neurochemically, and possibly functionally, although a double dissociation of function has not been shown. □

Received 20 May; accepted 1 July 1996.

1. Fritsch, G. & Hitzig, E. *Arch. Anat. Physiol. Wiss. Med.* **37,** 300–332 (1870).
2. Foerster, O. in *Handbuch der Neurologie* (eds Bumke, O. & Foerster, O.) 1–357 (Springer, Berlin, 1936).
3. Penfield, W. & Boldrey, E. *Brain* **60,** 389–443 (1937).
4. Woolsey, C. N. *et al. Res. Publ. Assoc. Res. Nerv. Ment. Dis.* **30,** 238–264 (1952).
5. Brodmann, K. *Vergleichende Lokalisationslehre der Grosshirnrinde* (Barth, Leipzig, 1909).
6. Strick, P. L. & Preston, J. B. *J. Neurophysiol.* **48,** 139–149 (1982).
7. Strick, P. L. & Preston, J. B. *J. Neurophysiol.* **48,** 150–159 (1982).
8. Kawashima, R. *et al. Neuroreport* **6,** 238–240 (1995).
9. Matelli, M., Luppino, G., Fogassi, L. & Rizzolatti, G. *J. Comp. Neurol.* **280,** 468–488 (1989).
10. Stepniewska, I., Preuss, T. M. & Kaas, J. H. *J. Comp. Neurol.* **330,** 238–271 (1993).
11. Stepniewska, I., Preuss, T. M. & Kaas, J. H. *J. Comp. Neurol.* **349,** 558–582 (1994).
12. Stepniewska, I., Preuss, T. M. & Kaas, J. H. *J. Comp. Neurol.* **349,** 536–557 (1994).
13. Schleicher, A. & Zilles, K. *J. Microsc.* **157,** 367–381 (1990).
14. Roland, P. E. & Zilles, K. *Trends Neurosci.* **17,** 458–467 (1994).
15. Schormann, T., von Matthey, M., Dabringhaus, A. & Zilles, K. *Bioimaging* **1,** 119–128 (1993).
16. Schormann, T., Dabringhaus, A. & Zilles, K. *IEEE Trans. Med. Imag.* **14,** 25–35 (1995).
17. Roland, P. E. *et al. Hum. Brain Map.* **1,** 173–184 (1994).
18. Roland, P. E. & Mortensen, E. *Brain Res. Rev.* **12,** 1–42 (1987).
19. Seitz, R. J., Roland, P. E., Bohm, C., Greitz, T. & Stone-Elander, S. *Eur. J. Neurosci.* **3,** 481–492 (1991).
20. Kunesch, E., Binkofski, F. & Freund, H. J. *Exp. Brain Res.* **78,** 539–546 (1989).
21. Merker, B. *J. Neurosci. Methods* **9,** 235–241 (1983).
22. Mahalanobis, P. C., Majumda, D. N. & Rao, C. R. *Sankhya Kalkutta* **9,** 89–324 (1949).
23. Zilles, K. & Schleicher, A. in *Autoradiography and Correlative Imaging* (eds Stumpf, W. & Solomon, H.) 277–307 (Academic, San Diego, 1995).
24. Roland, P. E. & Larsen, B. *Arch. Neurol.* **33,** 551–558 (1976).
25. Roland, P. E., Levin, B., Kawashima, R. & Åkerman, S. *Hum. Brain Map.* **1,** 3–19 (1993).

ACKNOWLEDGEMENTS. We thank K. Rascher for help with the manuscript. This work was supported by grants from the Swedish Medical Research Council, the Deutsche Forschungsgemeinschaft and the BioTech Programme.

CORRESPONDENCE and requests for materials should be addressed to K.Z. (e-mail: zilles@hirn.uni-duesseldorf.de).

Redistribution of synaptic efficacy between neocortical pyramidal neurons

Henry Markram & Misha Tsodyks

Department of Neurobiology, The Weizmann Institute for Science, Rehovot 76100, Israel

EXPERIENCE-dependent potentiation and depression of synaptic strength has been proposed to subserve learning and memory by changing the gain of signals conveyed between neurons[1,2]. Here we examine synaptic plasticity between individual neocortical layer-5 pyramidal neurons. We show that an increase in the synaptic response, induced by pairing action-potential activity in pre- and postsynaptic neurons, was only observed when synaptic input occurred at low frequencies. This frequency-dependent increase in synaptic responses arises because of a redistribution of the available synaptic efficacy and not because of an increase in the efficacy. Redistribution of synaptic efficacy could represent a mechanism to change the content, rather than the gain, of signals conveyed between neurons.

Changes in the amplitude of synaptic responses evoked by single-shock extracellular electrical stimulation of presynaptic fibres are usually considered to reflect a change in the gain of synaptic signals, and are the most frequently used measure for evaluating synaptic plasticity[1–5]. Synapses, however, do not merely transmit each action potential in an identical manner but do so in a manner which is dependent on the history of activity of the synapse[6]. It is therefore not possible to extrapolate from changes in single or even paired synaptic responses to the general behaviour of the synapse. To evaluate changes in the gain of a synapse it is necessary to consider the transmission of synaptic signals more complex than single excitatory postsynaptic potentials (e.p.s.ps) such as those evoked by a train of action potentials. Test synaptic responses evoked by high-frequency trains of extracellular electrical shocks may not only alter the sensitivity of axons to subsequent stimuli, but may also recruit polysynaptic circuits. It is therefore necessary to induce high-frequency transmission